Environ. Sci. Technol. **2010,** *44,* 8574–8580

An Improved Global Model for Air-Sea Exchange of Mercury: High Concentrations over the North Atlantic

ANNE L. SOERENSEN,[†,‡] ELSIE M. SUNDERLAND,[*,‡,§] CHRISTOPHER D. HOLMES,[‡] DANIEL J. JACOB,[‡] ROBERT M. YANTOSCA,[‡] HENRIK SKOV,[†] JESPER H. CHRISTENSEN,[†] SARAH A. STRODE,[∥] AND ROBERT P. MASON[⊥]

National Environmental Research Institute, Aarhus University, Frederiksborgvej 399, DK-4000 Roskilde, Denmark, School of Engineering and Applied Sciences and Department of Earth and Planetary Sciences, Harvard University, Cambridge Massachusetts 02138, United States, Department of Environmental Health, Harvard University School of Public Health, Boston Massachusetts 02115, United States, Department of Atmospheric Sciences, University of Washington, Seattle, Washington 98195, United States, and Department of Marine Sciences, University of Connecticut, 1080 Shennecossett Road, Groton, Connecticut, 0634, United States

Received June 15, 2010. Revised manuscript received October 1, 2010. Accepted October 7, 2010.

We develop an improved treatment of the surface ocean in the GEOS-Chem global 3-D biogeochemical model for mercury (Hg). We replace the globally uniform subsurface ocean Hg concentrations used in the original model with basin-specific values based on measurements. Updated chemical mechanisms for Hg^0/Hg^{II} redox reactions in the surface ocean include both photochemical and biological processes, and we improved the parametrization of particle-associated Hg scavenging. Modeled aqueous Hg concentrations are consistent with limited surface water observations. Results more accurately reproduce high-observed MBL concentrations over the North Atlantic (NA) and the associated seasonal trends. High seasonal evasion in the NA is driven by inputs from Hg enriched subsurface waters through entrainment and Ekman pumping. Globally, subsurface waters account for 40% of Hg inputs to the ocean mixed layer, and 60% is from atmospheric deposition. Although globally the ocean is a net sink for 3.8 Mmol Hg y^{-1}, the NA is a net source to the atmosphere, potentially due to enrichment of subsurface waters with legacy Hg from historical anthropogenic sources.

Introduction

Anthropogenic mercury (Hg) sources have enriched atmospheric Hg deposition globally by at least a factor of 3 (*1*). Atmospheric Hg is predominantly the gaseous elemental form (Hg^0), and is oxidized to Hg^{II}, which is then rapidly deposited. It is estimated that more than 80% of the Hg deposited to oceans is reemitted to the atmosphere as Hg^0, driving the cycle of Hg through biogeochemical reservoirs (*2*). Aqueous reduction of divalent inorganic mercury (Hg^{II}) and subsequent loss of Hg^0 reduces the potentially bioavailable Hg^{II} pool that may be converted to monomethylmercury, the most toxic species that poses health risks to fish consuming populations and wildlife (*3*).

Previous efforts to model Hg air−sea exchange (*2*) and atmospheric transport (*4*−*6*) have been unable to reproduce high atmospheric concentrations observed in the Northern Hemisphere marine boundary layer (MBL) during ocean cruises (*7*−*9*). We hypothesize that this results from subsurface seawater Hg enrichment, reflecting the legacy of past anthropogenic inputs and controlling Northern Hemisphere MBL concentrations. Previous research comparing preindustrial and contemporary Hg budgets for different ocean basins indicates that anthropogenic enrichment of Hg reservoirs in the Atlantic Ocean and Mediterranean Sea is >50% (*3*). Other regions such as deep waters of the Pacific Ocean have seen negligible anthropogenic impacts while Hg concentrations in intermediate waters of the North Pacific (NP) appear to be increasing (*10*). These gradients in subsurface Hg across ocean regions (*11, 12*) have not been represented in models simulating atmospheric Hg. Here we investigate the potential effects of legacy anthropogenic Hg accumulation on oceanic air−sea exchange in the GEOS-Chem global model (*1*) by including the effects of variability in subsurface ocean concentrations in our simulation.

Most marine surface waters are supersaturated in Hg^0 (*13, 14*). A combination of biologically mediated (*15*−*17*) and photochemical (*14, 18, 19*) processes reduce atmospherically deposited Hg^{II} in the water column to Hg^0. Field and laboratory studies suggest that photolytic processes drive most Hg^{II} reduction in surface waters but biotic reduction is also significant (*16, 17, 19*) and that aqueous Hg^0 oxidation involves reaction with photochemically produced $OH^•$ (*17, 20*). Oxidation rates appear to be enhanced in marine waters relative to freshwater (*21, 22*), possibly due the reaction of halides like Cl^- and Br^- with $OH^•$ to produce aqueous halogen radicals (*23*) or through the formation of stable Hg^{II} complexes that decrease reduction rates (resulting in greater net oxidation) (*17*).

The original slab-ocean model in GEOS-Chem (*2*) represents oceanic Hg cycling in a simplified manner using three rate coefficients that describe net reduction of atmospherically deposited Hg^{II}, conversion of Hg^{II} to nonreactive particulate Hg (Hg^P), and sinking of Hg^P. Each rate coefficient is adjusted to match observations. Here we update the chemical mechanisms for surface ocean Hg reactions to include both photochemical and dark Hg^0 oxidation, and both photolytic and biotic Hg^{II} reduction. We also model effects of light attenuation on redox reactions, Hg^{II} sorption to particles, and Hg^P removal from the surface layer based on export of organic carbon (*24*). We use the new model to investigate spatial and seasonal trends in oceanic Hg^0 evasion and the resulting Hg concentrations in the MBL.

Materials and Methods

General Model Description. GEOS-Chem, a global scale chemical transport model (CTM), was adapted for atmospheric and oceanic Hg cycling by Selin et al. (*5*) and Strode et al. (*2*). We use the most recent version of Holmes et al. (*25*), including Br atoms as the main atmospheric oxidant

* Corresponding author phone: +1-617-384-8832; e-mail: esunder@hsph.harvard.edu.
† Aarhus University.
‡ Harvard University.
§ Harvard University School of Public Health.
∥ University of Washington.
⊥ University of Connecticut.

10.1021/es102032g

Published on Web 10/25/2010

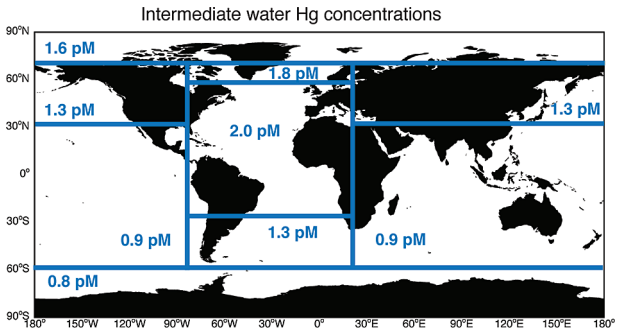

FIGURE 1. Subsurface ocean concentrations of inorganic Hg based on observations compiled by Sunderland and Mason (*24*), with recent measurement updates (*10, 34*).

for Hg^0. The model includes a 3-D atmospheric simulation (*5*), a 2-D surface-slab ocean simulation, and a 2-D dynamic terrestrial reservoir (*1*). We run simulations at 4° × 5° horizontal resolution with assimilated meteorological data for 2004−2008 from the NASA Goddard Earth Observing System (GEOS-5). Horizontal resolution of the surface ocean model is the same as the atmospheric model and the vertical depth varies depending on the monthly mixed layer depth (MLD) of the ocean (*26*). Three inorganic mercury forms are tracked by both the atmospheric and surface ocean simulations: Hg^{II}, Hg^0, and Hg^P.

Atmospheric Hg^{II} and Hg^P enter the surface ocean through wet and dry deposition. Anthropogenic Hg emissions are from the GEIA inventory for the year 2000 (*27*), adjusted for recent changes based on projections by Streets et al. (*28*). We reduced emissions from geogenic sources by 50% relative to those in Selin et al. (*1*) for consistency with recent global estimates for natural emissions (*29*). The model is spun-up to steady state for preindustrial conditions to equilibrate the 2-D terrestrial model and then updated to present-day by including anthropogenic emissions and increasing the terrestrial concentrations, following the procedure described by Selin et al. (*1*). The present-day simulation is then conducted for 5 years to equilibrate the surface ocean and the stratosphere. We use year 2008 for analysis.

Exchange with the Atmosphere and Subsurface Waters. Air−sea fluxes of Hg^0 are modeled using the parametrization of Nightingale et al. (*30*), the Henry's law coefficient for Hg^0 (*31*), a temperature-corrected Schmidt number for CO_2 (*32*), and the Wilke−Chang method for estimating a temperature and salinity-corrected Hg^0 diffusivity in different ocean regions (*33*) (see Supporting Information (SI) Table S4).

We retain vertical exchanges between the surface ocean and intermediate waters through entrainment/detrainment of the mixed layer and Ekman (wind-driven) pumping included in the original GEOS-Chem slab ocean model (*2*). Deepening of the surface ocean mixed layer (*26*) results in entrainment of Hg from intermediate waters and seasonal surface stratification results in detrainment.

The original GEOS-Chem slab ocean model (*2*) assumed a globally uniform subsurface ocean Hg concentration. We updated this (Figure 1) using observations compiled by Sunderland and Mason (*24*), and new data for the NP (*10*) and Arctic (*34*) Oceans. The model presently neglects lateral transport in surface currents and the vertical diffusion flux, which was a small constant (nonphysical) value in the Strode et al. (*2*) model. Both of these simplifications are areas for future model development.

Surface Ocean Redox Reactions. Our model incorporates separate terms for photolytic and biotic reduction, and photochemical and dark oxidation (Figure 2). We base the reducible fraction of the dissolved Hg^{II} pool on estimates from freshwater systems (*35*) and data indicating that stable chloride complexes abundant at high salinities are more resistant to reduction processes (*17, 36*). Reported ranges for the reducible pool from the above studies vary between approximately 40% and 60% of total Hg^{II} and we implement a value of 40% to best match the observational constraints provided by speciated surface ocean and atmospheric Hg concentrations (Figures 3 and 4). Re-equilibration of all reactive and nonreactive pools and Hg speciation occurs at each time step (60 min) in the model simulation.

Measured biotic Hg reduction rate coefficients in dark seawater incubation experiments range from 3.5×10^{-7} s^{-1} (*37*) to 8.3×10^{-5} s^{-1} (*18*). These experiments assume instantaneous equilibration of any added Hg to mimic Hg speciation under natural conditions (i.e., the rate coefficients apply only to the reducible Hg^{II} fraction). Many studies report relationships between biotic reduction rate coefficients in natural waters and factors such as productivity, particulate matter and bacterial activity (*17, 37, 38*). A variety of rate coefficient data for Hg^{II} photoreduction are also available (*16, 19, 21, 22, 39*). While these data provide guidance, most cannot be implemented directly in the model because they reflect net Hg^{II} reduction rate coefficients, are for unfiltered waters (do not isolate photoreduction and biotic reduction), and/or do not report radiation intensities.

We therefore used dual isotope addition data from Whalin et al. (*17*), who measured simultaneous photo-oxidation (k_{OX1}), photoreduction (k_{RED1}), and biotic reduction (k_{RED2}) rate coefficients (s^{-1}) in Chesapeake Bay seawater. By least-squares fit to the Whalin et al. (*17*) data, we derived linear relationships between total shortwave solar radiation (*R*, W

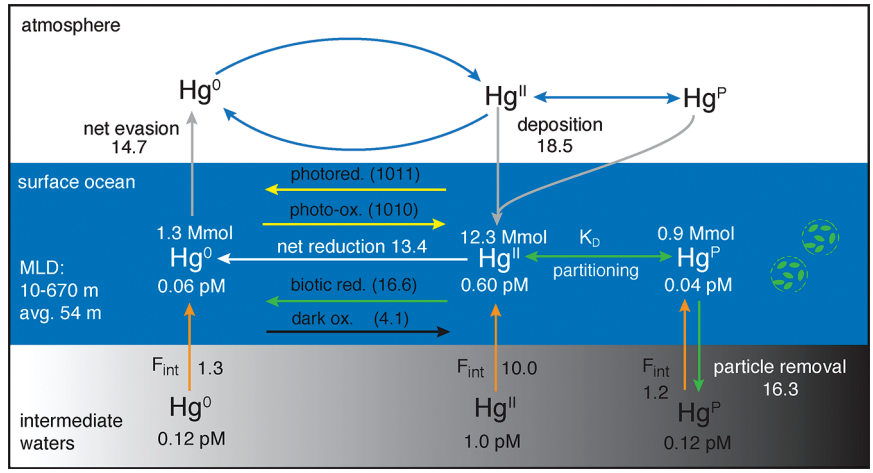

FIGURE 2. GEOS-Chem global budget of Hg in the surface ocean. Units are Mmol y^{-1} unless noted. F_{int} denotes net fluxes from intermediate waters through entrainment/detrainment of the mixed layer and Ekman pumping. MLD denotes mixing layer depth.

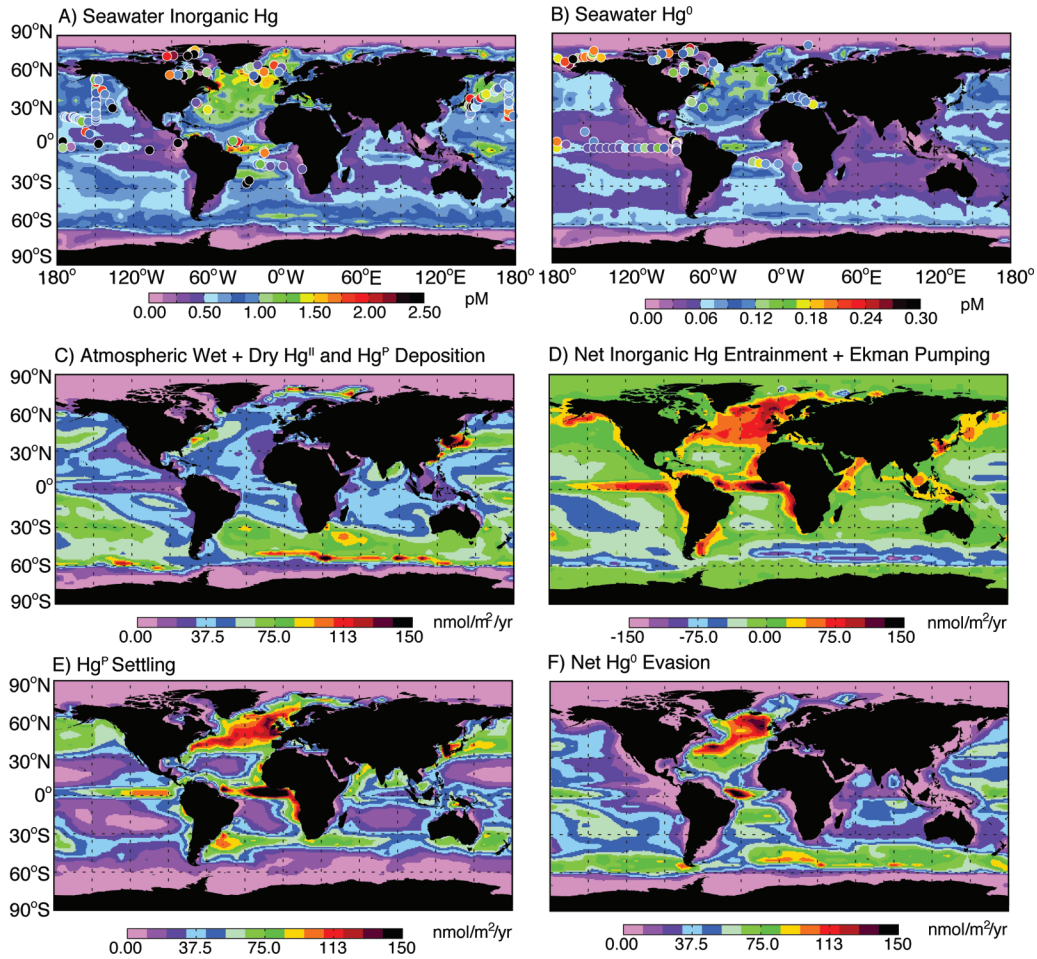

FIGURE 3. Global distribution of Hg concentrations and fluxes in the surface ocean. Fluxes and concentrations are annual mean values from the GEOS-Chem model simulation. Observed concentrations of total inorganic Hg and Hg^0 are shown as circles and include data from the Atlantic (*14, 45, 52, 53*); Pacific (*10, 12, 44, 54*); Arctic (*13, 34*). We omitted outliers in Hg^0 observations from two cruises in the Atlantic Ocean in the 1990s due to an apparent contamination problem (*14, 45*).

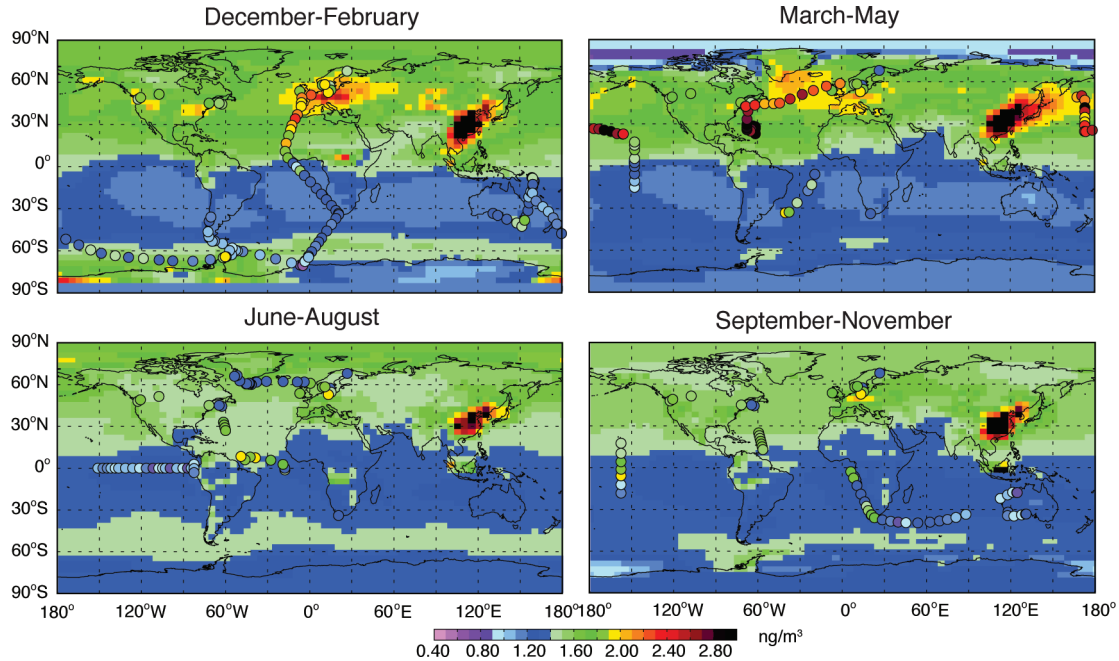

FIGURE 4. Mean Hg^0 concentrations in the atmospheric marine boundary layer (MBL) and terrestrial sites for different seasons. GEOS-Chem model values (background) are compared to cruise and land-based observations (circles) described in Kim and Fitzgerald (*54*), Soerensen et al. (*50*) and Selin et al. (*5*) and references therein.

m^{-2}), net primary productivity (NPP, gC m^{-2} d^{-1}) and k_{OX1}, k_{RED1}, and k_{RED2}. NPP values for this derivation were for the outer and shelf region of Chesapeake Bay characteristic of the measurement period (*40*). We further adjusted rate coefficients within observational confidence limits to be consistent with the ratio between photo-oxidation and photoreduction measured by Qureshi et al. (*39*), resulting in the following relationships implemented in our model: $k_{OX1} = 6.6 \times 10^{-6} \times R$; $k_{RED1} = 1.7 \times 10^{-6} \times R$; $k_{RED2} = 4.5 \times 10^{-6} \times NPP$. We also include a term for dark oxidation ($k_{OX2} = 1.0 \times 10^{-7}$ s^{-1}) based on Lalonde et al. (*21*).

Spatial and seasonal variability in redox rates are modeled based on light attenuation in the surface mixed layer, the surface local shortwave radiation flux from GEOS-5, and global NPP distributions from MODIS satellite data (*41*). Light attenuation with depth is estimated from empirically determined effective light absorption coefficients for seawater, dissolved organic carbon (DOC) and pigments, and their respective concentrations (*42*) (SI Table S3). Pigment concentrations are derived from MODIS satellite data, while DOC is based on a global mean of 1.5 mg L^{-1} in the surface mixed layer, scaled by the distribution of global NPP to account for productivity related concentration differences (*43*).

Sorption of Hg^{II} to Particles and Export Fluxes. We model Hg^P removal from the surface ocean by linking Hg^{II} sorption to particulate matter and settling to organic carbon export fluxes (the ocean biological pump). The affinity of aqueous Hg^{II} for the solid phase is described using an empirically measured partition coefficient (K_D, L kg^{-1}):

$$K_D = \frac{C_S}{C_D} \quad (1)$$

Where C_S is the suspended particlate matter (SPM) concentration of Hg^{II} on a dry weight (mass/mass) basis (pg kg^{-1}) and C_D is the filtered concentration (mass/volume) of Hg^{II} in seawater (pg L^{-1}). The model re-equilibrates the Hg^{II} pool between the dissolved and solid phases at each time step, prior to calculating the reducible and nonreducible dissolved Hg^{II} pools.

We use a log K_D value based on NP and North Atlantic (NA) measurements (5.5 ± 0.5) (*44, 45*). Since no global data sets for SPM concentrations in ocean surface waters are available, we use integrated water column algal biomass derived from MODIS chlorophyll a data and statistical relationships from Uitz et al. (*46*) for subsurface algal productivity (see SI Section II). Settling fluxes of Hg^P are calculated using the parametrization described in Sunderland and Mason (*24*) for export of particulate organic carbon with depth and Hg^P to carbon (Hg:C) ratios. Spatially and temporally variable Hg:C ratios are calculated at each time step in the model (global mean of 0.16 ng Hg per mg C) from the reservoir of Hg^P (derived from K_D) and the standing stock of organic carbon in the surface ocean (SI Table S2).

Results and Discussion

Global Budget. Figure 2 shows our global budget for Hg cycling in the surface ocean. Atmospheric deposition accounts for the largest fraction of Hg inputs to the surface ocean (18.5 Mmol y^{-1}). Entrainment of the mixed layer and Ekman pumping supply substantial amounts of Hg^{II} (10.0 Mmol y^{-1}), Hg^P (1.2 Mmol y^{-1}), and Hg^0 (1.3 Mmol y^{-1}) from intermediate waters, accounting for 40% (12.5 Mmol y^{-1}) of the global total Hg inputs to the surface ocean. Inputs are balanced by Hg^0 evasion (14.7 Mmol y^{-1}) and Hg^P removal (16.3 Mmol y^{-1}). Globally there is a net removal (sink) of 3.8 Mmol Hg y^{-1} to the subsurface ocean, mainly through particle-associated scavenging of Hg^P. Much of this Hg^P is remineralized in intermediate ocean waters.

Surface water Hg^0 reflects the supply of reducible Hg^{II} complexes and the rates of photolytic and biotic redox reactions. Turnover of the dissolved Hg^{II}/Hg^0 pools through photoreduction and photo-oxidation are rapid and dominate redox cycling except in environments where light is limited. Enhanced light penetration in oligotrophic areas with shallow mixed layers (e.g., seasonally in the Arctic, western Atlantic Ocean and western equatorial Pacific), means that photoreduction and photo-oxidation dominate dark redox processes where rate coefficients increase from a global mean 10^{-5} s^{-1} up to a maximum of 10^{-4} s^{-1} for reduction and 10^{-3} s^{-1} for oxidation. Biotic reduction is more important in highly productive regions (e.g., eastern Atlantic and eastern equatorial Pacific) where reaction rates increases from a global mean of 10^{-7} s^{-1} up to 10^{-6} s^{-1} and photo-oxidation and photoreduction decrease to 10^{-6} s^{-1} due to limited light penetration through the mixed layer.

Our modeled Hg^0 evasion falls within 90% confidence limits of previous estimates that ranged between 9.7 and 20.7 Mmol y^{-1} (*24*) and is in the same range as the previous GEOS-Chem ocean model (14.1 Mmol y^{-1}). Figure 2 shows the subsurface ocean contributes a substantial fraction of the Hg present in the mixed layer. These results contrast those of Strode et al. (*2*) who predicted that atmospheric deposition accounted for almost all (89%) of the Hg^{II} inputs. Better resolved intermediate water Hg concentrations in our simulation account for this difference.

Model Comparisons with Seawater Measurements. Figure 3A and B shows a comparison of modeled total Hg and Hg^0 in the global oceans with available surface ocean measurement data. Modeled seawater concentrations are highly variable ranging from <0.01 pM to >0.5 pM for Hg^0 and <0.1 pM to >2.5 pM for total Hg depending on month and region. Seawater measurements of aqueous total Hg and Hg^0 are extremely limited; thus data shown in Figure 3 span more than two decades compared to model results for 2008 (see also SI Figure S1−S2). Comparing model results from the Atlantic and Pacific Oceans with data from the decade preceding our simulation (1999−2008) reveals reasonable consistency with total Hg ($r = 0.95$) and Hg^0 ($r = 0.54$). However, there is little agreement between 2008 model results and measurements for the prior decade (1988−1998) of total Hg ($r = 0.24$) and Hg^0 ($r = -0.51$). Temporal trend data are insufficient to indicate whether these differences between observed (1988−1998) and modeled (2008) values are attributable to changes in environmental concentrations. The model does not capture elevated total Hg and Hg^0 concentrations measured in some coastal and shelf regions such as the Hudson Bay region (Figure 3A and B). The predicted coastal/shelf Hg concentrations may be low because the model does not presently include Hg inputs from rivers, which other modeling studies suggest substantially increase nearshore concentrations (*24, 47*). Additional model sensitivity analyses are described in the SI.

High Concentrations in the North Atlantic (NA) Ocean. Figure 3A and B show high concentrations of total Hg and Hg^0 in the NA. In addition to atmospheric deposition (Figure 3C), the NA receives large Hg contributions from subsurface waters through Ekman pumping and entrainment of intermediate waters (Figure 3D). Subsurface Hg entrainment is enhanced in the NA compared to other regions because wind-driven winter mixing increases the mixed layer depth from <50 m in the summer to over 600 m and intermediate waters are relatively enriched in Hg compared to other oceans (Figure 1). Sunderland and Mason (*24*) suggested that high relative Hg concentrations in NA subsurface waters (*12*) results from earlier peaks in anthropogenic emissions concentrated on the east coast of North America and Europe. Their results also showed a lag time of several decades in the NA before historical inputs are fully reflected by seawater

concentrations. Peaks in anthropogenic Hg emissions in the 1960−70s are evident in both sediment cores from eastern North America and historical inventories (e.g., refs *48, 49*).

Net Hg^0 evasion (Figure 3F) reflects the speed of air−sea exchange and Hg^0 supersaturation relative to the atmosphere. Combined Hg inputs and losses from the mixed layer (Figure 3C−3F) determine reducible Hg^{II} supply and Hg^0 concentrations. Although globally the ocean is a net Hg sink, much of the NA is a net source to the atmosphere (Figure 3F). In addition to large inputs from intermediate water entrainment, Ekman pumping and the speed of air−sea exchange are enhanced by high winds during winter months in the NA when losses from Hg^P settling are low (Figure 3E). Thus, much of the evaded Hg^0 likely originates from legacy Hg that has accumulated in subsurface waters.

Global Distribution of Hg^0 Evasion. Figure 2F shows the global distribution of modeled net annual Hg^0 evasion. The current simulation with atmospheric Hg^0 oxidation by Br atoms rather than OH/O_3 (*25*) shifts Hg^{II} deposition from the subtropics to high latitudes (Figure 3C). This shift results in higher evasion rates in the Southern Ocean, NA and NP relative to the previous simulation (*2*). Substantial Hg inputs to the mixed layer through entrainment and Ekman pumping are apparent in equatorial upwelling regions (Figure 3D), although these inputs are partially offset through losses by Hg^P settling (Figure 3E). Net losses through entrainment/detrainment and Ekman pumping (Figure 3D) occur in some areas of the South Pacific and Southern Ocean where subsurface Hg concentrations are lowest globally (Figure 1). Nutrient-like depletion of inorganic Hg concentrations occurs in highly productive regions of equatorial Atlantic (Figure 3E), which explains the low concentrations observed in this region (Figure 3A and B), and resulting low evasion rates.

Seasonal Variability in MBL Concentrations. Figure 4 shows simulated and observed Hg^0 concentrations in the atmospheric MBL for different seasons. Model results show the impacts of high NA ocean emissions (0.6 nmol m^{-2} d^{-1}) as peak MBL concentrations in the winter and early spring. In contrast, net Hg^0 deposition occurs during summer months (SI Figure S4). This pattern matches seasonal trends in monthly cruise measurements of MBL TGM concentrations ($r = 0.82$), as described by Soerensen et al. (*50*), that peak in the late winter and are lowest in the summer (Figure 5A).

Winter and early spring NA Hg^0 evasion rates are particularly high because of elevated Hg^{II} entrainment into the mixed layer, enhanced Ekman pumping, and high winds increase air−sea exchange rates (SI Figure S4). Conversely, in the summer and early fall mixed layer depth decreases (detrainment) and the reservoirs of Hg^0 and reducible Hg^{II} are more limited, lowering seawater Hg^0 saturation values relative to the atmosphere (SI Figure S4). In addition, enhanced productivity during summer months increases scavenging of Hg^P and can lower evasion by depleting the reducible Hg^{II} pool. Pronounced seasonality in NA oceanic evasion does not compromise the model's ability to capture trends at inland measurement sites (Figure 4), as discussed in Holmes et al. (*25*).

Enhanced modeled Pacific Ocean MBL concentrations are found primarily during the spring months, which also agrees with cruise measurements. However, oceanic emissions do not explain all elevated NP MBL observations (Figure 4). Seasonal differences in modeled NP Hg^0 evasion are not as pronounced due to lower subsurface Hg concentrations and less pronounced vertical mixing. For example, during winter months vertical mixing with intermediate waters accounts for 75% of Hg inputs to the NA surface waters compared to 30% for the NP. Elevated western NP MBL observations are therefore likely dominated by outflow from anthropogenic emissions in East Asia (*51*).

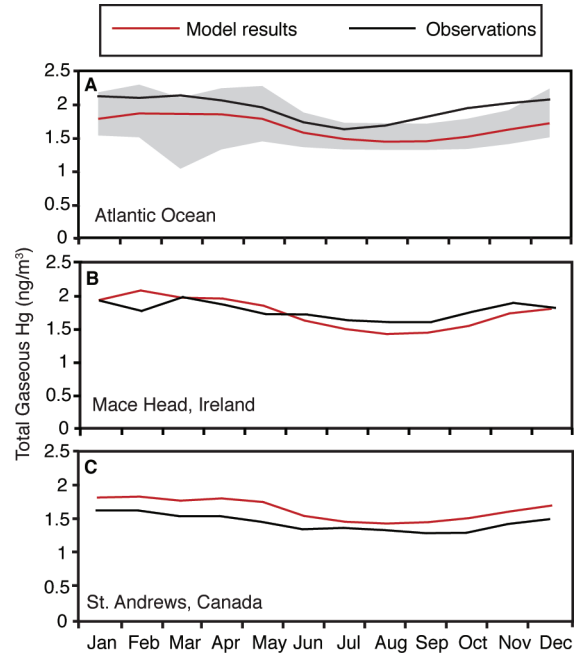

FIGURE 5. Seasonal variation of total gaseous Hg (TGM) in the marine boundary layer (MBL). Panel (A) shows the Atlantic Ocean (60:0W, 15:65N) and mean of all cruise measurements in the Atlantic. Gray areas indicate monthly maximum and minimum values. Panels (B) and (C) show values at the coastal sites Mace Head, Ireland and St. Andrews, Canada. Data sources are described in Soerensen et al. (*50*) and Selin et al. (*5*) and references therein.

Figure 5 compares the phase and amplitude of the seasonal cycle in MBL TGM concentrations with Atlantic Ocean measurements and selected coastal monitoring stations. The improved ocean model reproduces the seasonal cycle seen at most coastal monitoring sites (Birkenes, Pallas, Reiffel Island, Mace Head and St. Andrews) (e.g., Figure 5B and C). Both modeled and measured winter and spring MBL concentrations at marine stations shown in Figure 5 are higher than those seen at rural sites on the adjacent continents (*25*).

Results from our improved surface ocean model reinforce the importance of air−sea exchange processes as a control on MBL TGM concentrations. Oceanic emissions account for greater than 40% of MBL Hg levels in virtually all marine regions (SI Figure S5). Although the new model better captures seasonality and enhanced Northern Hemisphere MBL TGM concentrations relative to previous work (*2*), concentrations remain lower than some cruise measurements in the Atlantic Ocean (Figure 5A). Additional increases in evasion are not supported by model observational constraints based on terrestrial monitoring stations shown in Figure 4. We hypothesize that temporal changes in direct anthropogenic emissions and subsurface ocean concentrations has resulted in dynamic oceanic emissions and may help to explain observed MBL concentrations over the past two decades.

Acknowledgments

We acknowledge financial support for this work from the Electric Power Research Institute (EPRI), NERI-University of Aarhus, the Oticon Foundation, and the Hakun Lund foundation. R.P.M. acknowledges support from NSF Chemical Oceanography (OCE-728750). A.L.S. thanks Ole John Nielsen for mediating contact with SEAS, Harvard University.

Supporting Information Available

Additionl information including Figures S1−S5 and Tables S1−S4. This material is available free of charge via the Internet at http://pubs.acs.org.

Literature Cited

(1) Selin, N.; Jacob, D.; Yantosca, R.; Strode, S.; Jaegle, L.; Sunderland, E. Global 3-D land-ocean-atmosphere model for mercury: Present-day versus preindustrial cycles and anthropogenic enrichment factors for deposition. *Global Biogeochem. Cycles* **2008**, *22*, GB2011.

(2) Strode, S.; Jaegle, L.; Selin, N.; Jacob, D.; Park, R.; Yantosca, R.; Mason, R.; Slemr, F. Air-sea exchange in the global mercury cycle. *Global Biogeochem. Cycles* **2007**, *21*, GB1017.

(3) Sunderland, E. M. Mercury exposure from domestic and imported estuarine and marine fish in the U.S. seafood market. *Environ. Health Perspect.* **2007**, *115* (2), 235–242.

(4) Dastoor, A.; Larocque, Y. Global circulation of atmospheric mercury: a modelling study. *Atmos. Environ.* **2004**, *38*, 147–161.

(5) Selin, N. E.; Jacob, D. J.; Park, R. J.; Yantosca, R. M.; Strode, S.; Jaegle, L.; Jaffe, D. Chemical cycling and deposition of atmospheric mercury: Global constraints from observations. *J. Geophys. Res., [Atmos.]* **2007**, *112*, D02308.

(6) Seigneur, C.; Jayaraghavan, K.; Lohman, K.; Karamchandani, P.; Scott, C. Global source attribution for mercury deposition in the United States. *Environ. Sci. Technol.* **2004**, *38*, 555–569.

(7) Temme, C.; Slemr, F.; Ebinghaus, R.; Einax, J. Distribution of mercury over the Atlantic Ocean in 1996 and 1999−2001. *Atmos. Environ.* **2003**, *37*, 1889–1897.

(8) Slemr, F.; Brunke, E.-G.; Ebinghaus, R.; Temme, C.; Munthe, J.; Wangberg, I.; Schroeder, W.; Steffen, A.; Berd, T. Worldwide trend of atmospheric mercury since 1977. *Geophys. Res. Lett.* **2003**, *30* (10), 1516.

(9) Laurier, F.; Mason, R.; Whalin, L.; Kato, S. Reactive gaseous mercury formation in the North Pacific Ocean's marine boundary layer: a potential role of halogen chemistry. *J. Geophys. Res.* **2003**, *108* (D17), 4529.

(10) Sunderland, E. M.; Krabbenhoft, D. P.; Moreau, J. W.; Strode, S. A.; Landing, W. M. Mercury sources, distribution, and bioavailability in the North Pacific Ocean: Insights from data and models. *Global Biogeochem. Cycles* **2009**, *23*, Art. No. GB2010.

(11) Gill, G.; Fitzgerald, W. F. Vertical mercury distributions in the oceans. *Geochim. Cosmochim. Acta* **1988**, *52*, 1719–1728.

(12) Laurier, F.; Mason, R.; Gill, G.; Whalin, L. Mercury distribution in the North Pacific Ocean—20 years of observations. *Mar. Chem.* **2004**, *90* (1−4), 3–19.

(13) Andersson, M. E.; Sommar, J.; Gardfeldt, K.; Lindqvist, O. Enhanced concentrations of dissolved gaseous mercury in the surface waters of the Arctic Ocean. *Mar. Chem.* **2008**, *110* (3−4), 190–194.

(14) Mason, R.; Lawson, N.; Sheu, G.-R. Mercury in the Atlantic Ocean: factors controlling air-sea exchange of mercury and its distribution in upper waters. *Deep-Sea Res. II* **2001**, *48*, 2829–2853.

(15) Mason, R.; Rolfhus, K.; Fitzgerald, W. Methylated and elemental mercury cycling in surface and deep-ocean waters of the North Atlantic. *Water, Air, Soil Pollut.* **1995**, *80* (1−4), 665–677.

(16) Rolfhus, K. R.; Fitzgerald, W. F. Mechanisms and temporal variability of dissolved gaseous mercury production in coastal seawater. *Mar. Chem.* **2004**, *90* (1−4), 125–136.

(17) Whalin, L.; Kim, E.; Mason, R. Factors influencing the oxidation, reduction, methylation and demethylation of mercury species in coastal waters. *Mar. Chem.* **2007**, *107*, 278–294.

(18) Amyot, M.; Gill, G. A.; Morel, F. M. M. Production and loss of dissolved gaseous mercury in coastal seawater. *Environ. Sci. Technol.* **1997**, *31* (12), 3606–3611.

(19) Amyot, M.; Lean, D. R. S.; Poissant, L.; Doyon, M.-R. Distribution and transformation of elemental mercury in the St. Lawrence River and Lake Ontario. *Can. J. Fish. Aquat. Sci.* **2000**, *57* (Suppl. 1), 155–163.

(20) Gardfeldt, K.; Feng, X. B.; Sommar, J.; Lindqvist, O. In *Total Gaseous Mercury Exchange between Air and Water at River and Sea Surfaces in Swedish Coastal Regions*; Pergamon-Elsevier Science Ltd New York, 2001; pp 3027−3038.

(21) Lalonde, J.; Amyot, M.; Kraepiel, A.; Morel, F. Photooxidation of Hg(0) in artificial and natural waters. *Environ. Sci. Technol.* **2001**, *35*, 1367–1372.

(22) Lalonde, J. D.; Amyot, M.; Orvoine, J.; Morel, F. M. M.; Auclair, J. C.; Ariya, P. A. Photoinduced oxidation of Hg-0 (aq) in the waters from the St. Lawrence estuary. *Environ. Sci. Technol.* **2004**, *38* (2), 508–514.

(23) Zafiriou, O. C.; True, M. B.; Hayon, E., Consequences of OH radical reaction in sea water: Formation and decay of Br2- ion radical. In *Photochemistry of Environmental Aquatic Systems*; Zika, R. G., Cooper, W. J., Eds.; American Chemical Society: Washington, DC, 1987; pp 89−105.

(24) Sunderland, E. M.; Mason, R. Human impacts on open ocean mercury concentrations. *Global Biogeochem. Cycles* **2007**, *21*, GB4022.

(25) Holmes, C. D.; Jacob, D. J.; Corbitt, E. S.; Mao, J.; Yang, X.; Talbot, R.; Slemr, F. Global atmospheric model for mercury including oxidation by bromine atoms. *Atmos. Chem. Phys. Discuss.* **2010**, *10*, 19845−19900.

(26) Montegut, C. D.; Madec, G.; Fischer, A. S.; Lazar, A.; Iudicone, D. Mixed layer depth over the global ocean: An examination of profile data and a profile-based climatology. *J. Geophys. Res., [Oceans]* **2004**, *109* (C12), 20.

(27) Pacyna, E.; Pacyna, J.; Steenhuisen, F.; Wilson, S. Global anthropogenic mercury emission inventory for 2000. *Atmos. Environ.* **2006**, *40*, 4048–4063.

(28) Streets, D. G.; Zhang, Q. Projections of global mercury emissions in 2050. *Environ. Sci. Technol.* **2009**, *43* (8), 2983–2988.

(29) Pirrone, N.; Cinnirella, S.; Feng, X.; Finkelman, R.; Friedli, H. R.; Leaner, J.; Mason, R. P.; Mukherjee, A. B.; Stracher, G.; Streets, D. G.; Telmer, K. Global mercury emissions to the atmosphere from anthropogenic and natural sources. *Atmos. Chem. Phys. Discuss.* **2010**, *10*, 4719–4752.

(30) Nightingale, P.; Malin, G.; Law, C.; AJ, W.; Liss, P.; Liddicoat, M.; Boutin, J.; Upstill-Goddard, R. In situ evaluation of air-sea gas exchange parameterizations using novel conservative and volatile tracers. *Global Biogeochem. Cycles* **2000**, *14* (1), 373–387.

(31) Andersson, M. E.; Gardfeldt, K.; Wangberg, I.; Stromberg, D. Determination of Henry's law constant for elemental mercury. *Chemosphere* **2008**, *73* (4), 587–592.

(32) Poissant, L.; Amyot, M.; Pilote, M.; Lean, D. Mercury water-air exchange over the upper St. Lawrence River and Lake Ontario. *Environ. Sci. Technol.* **2000**, *2000* (34), 3069–3078.

(33) Wilke, C. R.; Chang, P. Correlation of diffusion coefficients in dilute solutions. *AIChE J.* **1955**, *1* (2), 264–270.

(34) Kirk, J. L.; St. Louis, V.; Hintelmann, H.; Lehnherr, I.; Else, B.; Poissant, L. Methylated mercury species in marine waters of the Canadian High and Sub Arctic. *Environ. Sci. Technol.* **2008**, *42* (22), 8367–8373.

(35) O'Driscoll, N.; Siciliano, S.; Lean, D.; Amyot, M. Gross photoreduction kinetics of mercury in temperate freshwater lakes and rivers: Application to a general model of DGM dynamics. *Environ. Sci. Technol.* **2006**, *40*, 837–843.

(36) Stumm, W.; Morgan, J. J., *Aquatic Chemistry: Chemical Equilibria and Rates in Natural Waters*, 3rd ed. ; John Wiley & Sons, Inc.: New York, NY, 1996; p 1022.

(37) Mason, R. P.; Morel, F. M. M.; Hemond, H. F. The role of microorganisms in elemental mercury formation in natural waters. *Water, Air, Soil Pollut.* **1995**, *80*, 775–787.

(38) Poulain, A. J.; Ni Chadhain, S. M.; Ariya, P. A.; Amyot, M.; Garcia, E.; Campbell, P. G. C.; Zylstra, G. J.; Barkay, T. Potential for mercury reduction by microbes in the high arctic. *Appl. Environ. Microbiol.* **2007**, *73* (7), 2230–2238.

(39) Qureshi, A.; O'Driscoll, N. J.; MacLeod, M.; Neuhold, Y. M.; Hungerbuhler, K. Photoreactions of mercury in surface ocean water: gross reaction kinetics and possible pathways. *Environ. Sci. Technol.* **2010**, *44* (2), 644–649.

(40) Cerco, C. Phytoplankton kinetics in the Chesapeake Bay Eutrophication Model. *Water Qual. Ecosyst. Model.* **2000**, *1*, 5–49.

(41) Behrenfeld, M. J.; Falkowski, P. G. Photosynthetic rates derived from satellite-based chlorophyll concentration. *Limnol. Oceanogr.* **1997**, *42* (1), 1–20.

(42) Wozniak, B.; Dera, J., *Light Absorption in Sea Water*; Springer: New York, NY, 2007; p 456.

(43) Chester, R., *Marine Geochemistry*, 2nd Ed.; Blackwell Science Ltd.: Berlin, Germany, 2003; p 506.

(44) Mason, R. P.; Fitzgerald, W. The distribution and cycling of mercury in the equatorial Pacific Ocean. *Deep-Sea Res., Part 1* **1993**, *40* (9), 1897–1924.

(45) Mason, R.; Rolfhus, K.; Fitzgerald, W. Mercury in the North Atlantic. *Mar. Chem.* **1998**, *61*, 37–53.

(46) Uitz, J.; Claustre, H.; Morel, A.; Hooker, S. B. Vertical distribution of phytoplankton communities in open ocean: An assessment based on surface chlorophyll. *J. Geophys. Res., [Oceans]* **2006**, *111* (C8), 23.

(47) Sunderland, E. M.; Dalziel, J.; Heyes, A.; Branfireun, B. A.; Krabbenhoft, D. P.; Gobas, F. Response of a macrotidal estuary to changes in anthropogenic mercury loading between 1850 and 2000. *Environ. Sci. Technol.* **2010**, *44* (5), 1698–1704.

(48) Sunderland, E. M.; Cohen, M.; Selin, N.; Chmura, G. Reconciling models and measurements to assess trends in atmospheric mercury deposition. *Environ. Pollut.* **2008**, *156*, 526–535.
(49) Sunderland, E. M.; Chmura, G. L. An inventory of historical mercury pollution in Maritime Canada: Implications for present and future contamination. *Sci. Total Environ.* **2000**, *256* (1), 39–57.
(50) Soerensen, A. L.; Skov, H.; Jacob, D. J.; Soerrensen, B. T.; Johnson, M. S., Global concentrations of gaseous elemental mercury and reactive gaseous mercury in the marine boundatry layer. *Environ. Sci. Technol.* **2010**, *44*, 7425−7430.
(51) Strode, S.; Jaegle, L.; Jaffe, D.; Swartzendruber, P.; Seline, N.; Holmes, C.; Yantosca, R., Trans-Pacific transport of mercury. *J. Geophys. Res., [Atmos.]* **2008**, *113*, D15305, DOI: 10.1029/2007JD009428.
(52) Mason, R.; Sullivan, K. A. The distribution and speciaiton of mercury in the South and equatorial Atlantic. *Deep-Sea Res., Part II* **1999**, *46*, 937–956.
(53) Lamborg, C. H.; Hammerschmidt, C. R.; Saito, M.; Goepfert, T.; Lam, P. J., Mercury methylation in the gyre and benguela upwelling regions of the tropical south atlantic ocean. In *9th International Conference on Mercury as a Global Pollutant*; Guiyang, China, June 7−12, 2009.
(54) Kim, J.; Fitzgerald, W. Sea-Air partitioning of mercury in the equatorial Pacific Ocean. *Science* **1986**, *231* (4742), 1131−1133.

ES102032G